Deviations of the exciton level spectrum in Cu_2O from the hydrogen series

F. Schöne, S.-O. Krüger, P. Grünwald, H. Stolz, and S. Scheel
Institut für Physik, Universität Rostock, Albert-Einstein-Strasse 23, D-18059 Rostock, Germany

M. Aßmann, J. Heckötter, J. Thewes, D. Fröhlich, and M. Bayer
Experimentelle Physik 2, Technische Universität Dortmund, D-44221 Dortmund, Germany

Recent high-resolution absorption spectroscopy on excited excitons in cuprous oxide [Nature **514**, 343 (2014)] has revealed significant deviations of their spectrum from that of the ideal hydrogen-like series. Here we show that the complex band dispersion of the crystal, determining the kinetic energies of electrons and holes, strongly affects the exciton binding energies. Specifically, we show that the nonparabolicity of the band dispersion is the main cause of the deviation from the hydrogen series. Experimental data collected from high-resolution absorption spectroscopy in electric fields validate the assignment of the deviation to the nonparabolicity of the band dispersion.

PACS numbers: 71.35.Cc, 78.20.-e, 32.80.Ee, 33.80.Rv

arXiv:1511.05458v2 [cond-mat.mes-hall] 22 Feb 2016

I. INTRODUCTION

Fluorescence spectra of atomic systems are an extremely rich source of information about the interactions of electrons and the nuclei, and their study laid the foundations of the development of quantum mechanics. The basic hydrogen dependence of the electron binding energies of $1/n^2$ already turns out to be insufficient for alkali, i.e. hydrogen-like, atoms where the polarisability of the ionic core modifies the Coulomb potential felt by the valence electron. In semiconductor physics, the exciton concept translates the bound states of an electron-hole pair onto a hydrogen-like series, where the crystal environment is included in the effective masses and the dielectric function of the material [1–3]. However, the periodic arrangement of the crystal constituents breaks the rotational symmetry of atoms, and leads to semiconductor-specific effects such as detailed level splittings [4]. These splittings demonstrate deviations from the Rydberg formula.

Here we calculate the correct binding energies of Cu_2O from the band structure and cast them into the form of single-parameter corrections to the Rydberg series. In contrast to atoms, the origin of the excitonic correction is not a modification of the Coulomb potential, but the deviation from the parabolic band dispersion and hence the kinetic energy of electrons and holes. Based on the group-theoretical band Hamiltonian of Suzuki and Hensel (SH) [5] adapted to the exact band structure of cuprous oxide derived using density functional theory [6],we compute the exciton binding energies and extract from them the relevant corrections to the Rydberg series. Our theoretical results are compared to experimental data collected by high-resolution absorption spectroscopy. In combination with electric fields, we are able to extract the binding energies of excitons of S-, P-, D- and F-type, extending previous studies to far higher principal quantum numbers. The excellent agreement between theory and experiment corroborates our assignment of the deviations of the exciton level spectrum to the nonparabolicity of the band dispersion.

II. VALENCE BAND DISPERSIONS IN CUPROUS OXIDE

Cuprous oxide (Cu_2O) was historically the first material in which excitons were observed [7–9]. Their discovery, combined with the availability of exceptionally pure natural crystals [10], sparked considerable interest in light-matter interactions in condensed-matter systems. Cuprous oxide is endowed with a relatively large Rydberg energy of around 86 meV. The crystal environment is taken into account by the permittivity ε that, for crystals with cubic (O_h) symmetry such as Cu_2O, is typically isotropic. This means that the exciton spectrum should simply be a scaled hydrogen spectrum. However, recent high-precision measurements of the P-exciton energies of the yellow series of Cu_2O showed a systematic deviation of the observed spectrum from the hydrogen analogy expectation [11], in addition to the splitting of the excitons with different angular momenta for low n [4]. Several effects such as the influence of a frequency- and wavevector-dependent permittivity $\varepsilon(\mathbf{k},\omega)$, the coupling to LO-phonons as well as exchange interactions have all been proposed as causes for that deviation [12]. In two-dimensional materials such as transition metal dichalgogenides (TMDC), the nonlocal nature of the Coulomb screening causes similar effects [13–15]. However, as we will show here, the deviation of the exciton binding energies of the yellow series in bulk cuprous oxide from the hydrogenic Rydberg series is a result of the nonparabolic dispersion of the highest valence band (with symmetry Γ_7^+ at the Brillouin zone center).

The description of excitons in a semiconductor requires the detailed knowledge of the electronic band structure. The common approach in solid-state physics is to approximate the extrema of valence and conduction bands via parabolic shapes. In the effective mass approximation these parabolas are then interpreted as the kinetic energy terms of electron and hole, respectively. A simple

two-band model yields the Wannier equation, which is analogous to the Schrödinger equation for hydrogen, and whose bound state solutions are the excitons [16] following the simple Rydberg formula.

Additional interactions such as spin-orbit and interband interactions lead to further splitting and deformation of the relevant bands under consideration. In Cu_2O, the highest valence band with symmetry Γ_5^+ splits under the spin-orbit interaction $\mathcal{H}_{\rm so} = \frac{1}{3}\Delta\,(\mathbf{I}\cdot\boldsymbol{\sigma})$, where $\mathbf{I}$ denotes the angular-momentum matrices for $I = 1$ and $\boldsymbol{\sigma}$ the Pauli spin matrices, into one (doubly degenerate) Γ_7^+- and two (doubly degenerate) Γ_8^+-bands, associated with total angular momenta $J = 1/2$ and $J = 3/2$, respectively [5]. The value of the spin-orbit splitting in Cu_2O is $\Delta = 131$ meV. From symmetry arguments [17] it follows that band interactions can be taken into account in a 6×6-matrix Hamiltonian that includes powers of the momentum $\mathbf{k}$ up to second order [5],

$$\mathcal{H}_k = \frac{\hbar^2}{2m_e}\Bigg(\left[A_1 + B_1(\mathbf{I}\cdot\boldsymbol{\sigma})\right]k^2 + \left[A_2\left(I_x^2 - \frac{1}{3}I^2\right) + B_2\left(I_x\sigma_x - \frac{1}{3}\mathbf{I}\cdot\boldsymbol{\sigma}\right)\right]k_x^2 + \text{c.p.} + \left[A_3(I_xI_y + I_yI_x) + B_3(I_x\sigma_y + I_y\sigma_x)\right]\{k_xk_y\} + \text{c.p.}\Bigg), \tag{1}$$

where c.p. stands for cycling permutations and $\{k_xk_y\} = (k_xk_y + k_yk_x)/2$. The band interaction Hamiltonian $\mathcal{H}_k$ contains a total of six dimensionless parameters $\{A_{1\cdots3}, B_{1\cdots3}\}$, which can be obtained by matching the resulting energy dispersions to the exact band structure derived from spin-DFT calculations [6]. Note that DFT does not give the correct gap energy, which can be obtained experimentally.

The fit was performed for the highest valence band (Γ_5^+) which splits due to the spin-orbit interaction into an energetically higher Γ_7^+ and the two lower-energy Γ_8^+ bands. This yields three individual energy dispersions $E_{SH}^{(i)}(\mathbf{k})$ ($i = 7, 8hh, 8lh$) for each direction in the Brillouin zone. A least-squares fit to the Γ_7^+ band that is of interest to us yields the parameters $A_1 = -1.76$, $A_2 = 4.519$, $A_3 = -2.201$, $B_1 = 0.02$, $B_2 = -0.022$, and $B_3 = -0.202$. The lowest conduction band (Γ_6^+) can easily be approximated by a parabola in the vicinity of the Γ-point and it has an isotropic curvature in all directions. The bound states formed between the Γ_6^+ and the Γ_7^+, Γ_8^+ bands are the excitons of the yellow and green series, respectively. Figure 1 shows the relevant bands and the fits to the Hamiltonian $\mathcal{H}_{\rm SH} = \mathcal{H}_{\rm so} + \mathcal{H}_k$. In the following, we neglect the anisotropy of the band dispersions and use a weighted average $\overline{E}_{SH}^{(i)}$ for simplicity, with the weights being the respective geometric multiplicities. After this procedure, there is no free parameter left. Furthermore, in doing so, the exciton angular momentum $l = 0, 1, 2, \ldots$ becomes a good quantum number for labelling the states. Tiny fine structure splittings as reported recently are neglected [18].

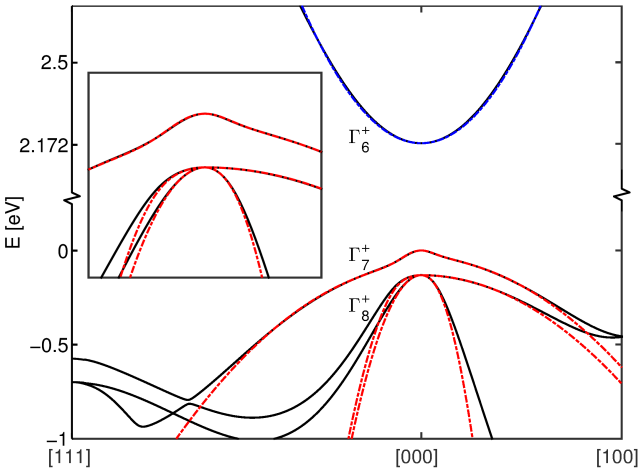

FIG. 1: Relevant band dispersions along two particular directions in the Brillouin zone. Black lines: band dispersions from spin-DFT [6]. Blue dashed line: parabolic model for the lowest conduction (Γ_6^+) band with an effective electron mass $m_e^* = 0.98\,m_e$. Red dashed lines: best fits of the dimensionless parameters $\{A_{1\cdots3}, B_{1\cdots3}\}$ in $\mathcal{H}_k$ [Eq. (1)] to the band structure. The inset shows the uppermost valence bands and the corresponding fits in the vicinity of the Γ-point.

III. EXCITON BINDING ENERGIES

In the following we restrict our analysis to the excitons of the yellow series ($\Gamma_6^+\otimes\Gamma_7^+$) while an investigation of the excitons of the green series ($\Gamma_6^+\otimes\Gamma_8^+$) would follow a similar path. We first split the valence band dispersion $\overline{E}_{SH}^{(7)}$ into a parabolic part T_h near $\mathbf{k} = \mathbf{0}$ and a nonparabolic contribution $\Delta T_h(k_h)$. Adding the kinetic energy T_e of the conduction band as well as the Coulomb interaction V_{e-h} to the valence band dispersion results in a Wannier equation that, due to the nonparabolic valence band dispersion, no longer resembles a simple Schrödinger-type equation. After transformation to the single-particle (exciton) picture and neglecting the center-of-mass momentum (i.e. setting $\mathbf{K} = \mathbf{0}$), the Hamiltonian takes the general form

$$\mathcal{H} = \frac{\hbar^2k^2}{2\mu} + \Delta T_h + V_{e-h}(\mathbf{k})\star \tag{2}$$

with the reduced exciton mass μ defined as usual. Here, the symbol $\star$ denotes the convolution operator.

The exciton binding energies $E_{n,l}$ are then obtained from the eigenvalue equation $\mathcal{H}\Phi(\mathbf{k}) = E_{n,l}\Phi(\mathbf{k})$ in momentum space which, due to the convolution with the Coulomb potential, is in fact an integral equation. Without the nonparabolic contribution ΔT_h, the solution for the momentum-space wavefunction $\Phi(\mathbf{k})$ is that for hydrogenic systems [19], and the energy eigenvalues $E_{n,l}$

follow a hydrogen-like Rydberg series. Inclusion of the term ΔT_h prevents one from obtaining an analytic solution.

In this case, we make use of a method proposed in Ref. [20] by which the original eigenvalue problem $\mathcal{H}\Phi(\mathbf{k}) = E_{n,l}\Phi(\mathbf{k})$ is converted into an auxiliary Sturmian eigenvalue problem

$$\left(\frac{\hbar^2 k^2}{2\mu} + \Delta T_h - E_{n,l}\right)\Phi(\mathbf{k}) = -\lambda(E_{n,l})V_{e-h}(\mathbf{k}) \star \Phi(\mathbf{k}) \tag{3}$$

with Sturmian eigenvalue $\lambda(E_{n,l})$ that itself depends parametrically on the sought energy eigenvalue $E_{n,l}$. The energy eigenvalues of the system now emerge from the λ-spectrum if the condition $\lambda(E_{n,l}) = 1$ is met. The advantage of this method is that Eq. (3) can be transformed, after separation of radial and angular variables, into a Fredholm integral equation of the second kind, whose real and symmetric integral kernel can be spectrally decomposed into eigenfunctions $g_{n,l}(k)$.

In the absence of any nonparabolicity ($\Delta T_h = 0$), the eigenfunctions $g_{n,l}(k)$ are orthonormal, and the condition $\lambda(E_{n,l}) = 1$ yields the standard hydrogenic Rydberg formula [20]. The inclusion of ΔT_h results in a mixing of eigenfunctions $g_{n,l}(k)$ with different principal quantum numbers n. Therefore, an additional diagonalisation step has to be added. The numerical procedure thus involves:

1. solving the integral equation (3) for all principal quantum numbers n with $n \leq n_{\max}$ for a given angular quantum number l, with $E_{n,l}$ as parameters,
2. diagonalising the matrix of (non-orthogonal) eigenfunctions $g_{n,l}(k)$,
3. and extracting the energy eigenvalues that fulfil the condition $\lambda(E_{n,l}) = 1$.

Typically, principal quantum numbers up to $n_{\max} = 60$ provided good convergence of the numerical procedure to obtain the exciton spectrum up to $n = 25$.

IV. DEVIATION FROM THE RYDBERG SERIES

The energy eigenvalues $E_{n,l}$ that are obtained from such a diagonalisation do no longer follow the Rydberg series of a hydrogen atom. In semiconductor physics, the common approach at this point is to employ $\mathbf{k}\cdot\mathbf{p}$-theory to account for the nonspherical symmetry [21–23]. Incorporating the Luttinger parameters of Cu_2O, it allows one to determine the binding energies as demonstrated in Ref. [18]. However, a few remarks are in order in comparison to our approach. Besides the band gap and the Rydberg-energy, applying $\mathbf{k}\cdot\mathbf{p}$-theory to cuprous oxide requires the Luttinger parameters and in some cases the dielectric function, which are both determined by fitting the model Hamiltonian to the experimental band structure. In contrast, our approach fits the most general Hamiltonian for the cubic crystal symmetry to an ab initio calculation of the band structure, thus avoiding any experimental fit parameters at this point. Furthermore, the solution of the coupled differential equations in the $\mathbf{k}\cdot\mathbf{p}$-approach requires a set of basis functions that are arbitrary at this point. On the other hand, the structure of the Fredholm integral equation yields a natural basis set $g_{n,l}$. Another advantage of our method is that we describe one source of deviations at one time. Combined with our purely theoretical data we are thus able to gauge the influence of the nonparabolicity on the deviation of exciton binding energies from the Rydberg series.

Phenomenologically, the energy shift of the excitonic Rydberg series can also be traced back to deviations of the interaction potential between electron and hole from the strict Coulomb potential at short distances (central-cell corrections). For excitons in Cu_2O this was done for the first time in Ref. [24]. There, the atomic concepts of quantum defects was applied, but only to match experimental data of the yellow S-excitons, with the assumption that the quantum defect for the P-excitons is negligibly small. Besides the nonparabolicity of the bands, the binding energy of the excitons can be affected by other central-cell corrections such as the coupling of electrons and holes to LO-phonons, the frequency-dependent dielectric function $\varepsilon(\mathbf{k},\omega)$ and exchange interactions [12]. However, as we are interested in excitons with large principal quantum number n, their low binding energy prevents the coupling to LO-phonons. Possible coupling to phonons above the band gap is suppressed due the limitation of phonons by the low temperature. In addition, a large exciton Bohr radius allows one to assume that the dielectric function can be treated as a constant $\varepsilon = 7.5$ [25], hence we expect the contribution of the other central-cell corrections to be negligibly small. Overall, one may expect the nonparabolicity of the valence to be the major source of corrections to the ideal Rydberg series.

As the deviations from the ideal Rydberg series are small compared to the binding energies and tend to zero for large n, it is convenient to display these corrections relative to ideal variations of binding energies as

$$\alpha_{n,l} = \left|\frac{E_n - E_n^*}{E_{n+1}^* - E_n^*}\right|, \tag{4}$$

where E_n is the actually measured binding energy (difference to band gap), while the E_ν^* represent ideal Rydberg energies Ry/ν^2. The results are shown in Fig. 2 (solid lines) as function of principal quantum number n for the lowest angular momentum states with $l = 0\ldots3$. As expected from the modified Hamiltonian (2), the theoretical corrections saturate for large n, and decrease with increasing l.

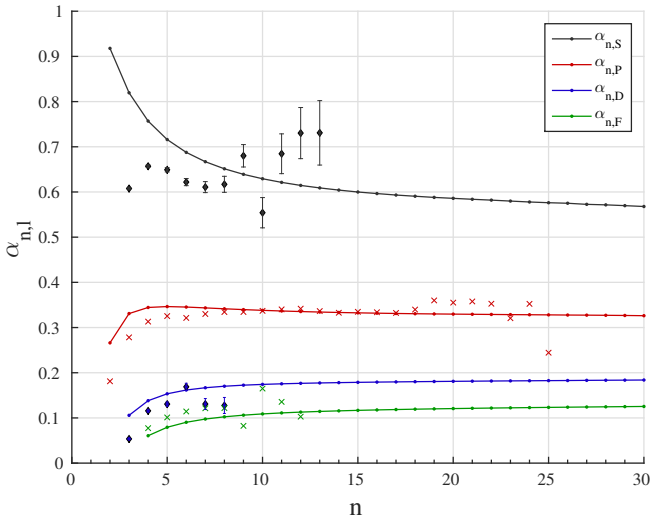

FIG. 2: Deviations $\alpha_{n,l}$ from the Rydberg series of the yellow excitons in Cu_2O as function of principal quantum number n for angular momenta $l = 0 \ldots 3$. Solid lines: energy eigenvalues from Eq. (3). Marker: experimental values (S – black dots, P – red crosses, D – blue dots, F – green crosses) from absorption spectroscopy.

V. TRANSMISSION SPECTROSCOPY

To determine the energies of exciton states in Cu_2O experimentally, we performed high resolution absorption spectroscopy on a high-quality crystal. The energies of the P-excitons can be accessed directly by one-photon absorption in electric-dipole approximation, as demonstrated in [11]. In a strict sense angular momentum is not a good quantum number in crystals, but can be used approximately in high-symmetry cubic crystals with O_h or T_d symmetry. The symmetry reduction leads to an admixture of P-excitons to the F-excitons so that they become observable in absorption [4]. As a consequence, the energies of these states can be determined with high accuracy [18]. In case they show a fine structure splitting, we have taken the center of gravity energy of the corresponding multiplet, which is in line with the theoretical model that averages over different k-space directions. While the energies of excitons with odd-parity envelopes can be determined accurately in that way, this is not possible for states with even parity.

Therefore, we applied additionally an electric field along the optical axis, which leads to a mixing of the S-exciton with the P-exciton with zero magnetic quantum number. Similarly, D-excitons become mixed with P- and F-excitons of the same magnetic quantum number. As a consequence, the related features appear in the absorption spectra, see Fig. 3, which shows the absolute absorption of the $n = 4$ and $n = 5$ excitons as function of the electric field. With increasing field strength new features emerge and intensify, as expected from the increased state mixing with the P-excitons. Also line splittings are observed which ultimately lead to the Stark ladder. From extrapolation towards $U = 0$, the energies of these excitons at zero field can be accurately assessed. From their order in energy we can attribute them to S- and P-excitons, as labeled.

To enhance the accuracy of the energy evaluation, we have also taken the second derivatives of the absorption spectra, shown in Fig. 4. By doing so, the enormous intensity differences in absolute transmission are leveled out, and the different absorption lines become much better resolvable, so that high-accuracy determination of the S- and D-exciton energies becomes possible: For the D-excitons again the center-of-gravity is determined for each principal quantum number. In doing so, we are able to extend the reported energies to significantly higher principal quantum numbers, for the S-excitons up to $n = 12$ compared to 7 in previous reports, and up to $n = 8$ for the D-excitons compared to 5 previously. The assignment of the states via the second derivative is depicted in the transmission spectrum Fig. 3 by the dotted lines. Note that for higher n these excitons become also optically activated in electric fields. However, it is no longer possible to assign them in the multiplicity of emerging lines, so that also their energies can no longer be determined with the required accuracy for assessing the deviation $\alpha_{n,l}$.

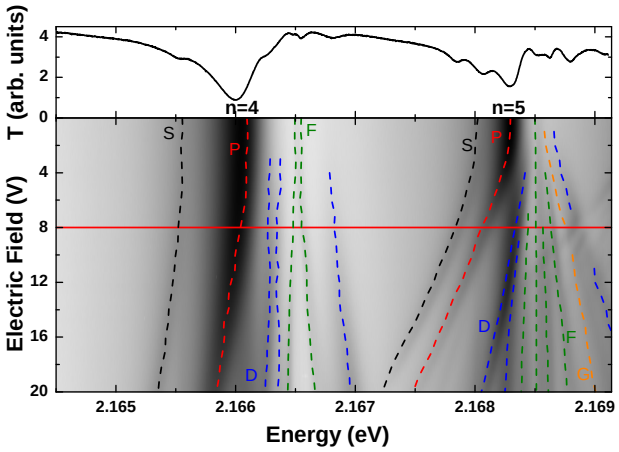

FIG. 3: Absorption spectra of the $n = 4$ and $n = 5$ excitons in external electric fields. The curve on top shows a cut through the contour plot at $U = 8$ V.

VI. RESULTS AND DISCUSSION

The experimentally extracted values for the deviations $\alpha_{n,l}$ of the exciton binding energies from the ideal Rydberg series are shown in Fig. 2, together with the theoretical results for the energy eigenvalues that are obtained from solving Eq. (3). In addition, the S-excitons are affected by electron-hole exchange interaction with a common scaling of n^{-3}. The experimental binding energies

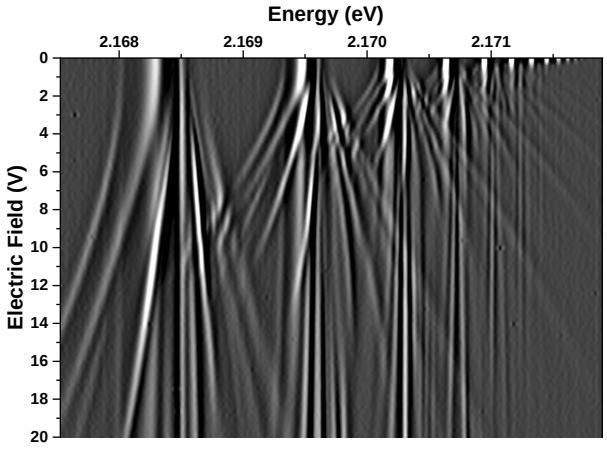

FIG. 4: Contour plot of the second derivative of an absorption spectrum extended over a larger energy range covering the excitons from $n = 5$ towards the band gap. The multiple splitting of the states while transforming into the Stark ladder becomes obvious.

of the S-excitons, whose deviation $\alpha_{n,S}$ is depicted in Fig. 2, have thus been shifted downwards by an amount of 8.04 meV/n^3 (following previous measurements of the exchange [4]) with respect to the values extracted from the absorption spectra.

The agreement, in particular of the P-exciton resonances for large n, is astonishingly good. This implies that nonparabolicity of the bands (in case of Cu_2O only the valence bands) due to interband coupling is the dominant contribution to the deviation of the exciton resonances from the hydrogenic Rydberg series. Nonetheless, one still observes a systematic deviation of the S-exciton energies from their predicted values, in particular for low n. This can be attributed to the fact that in this energy range the background permittivity $\varepsilon(\mathbf{k}, \omega)$ is far from constant [26], and that the binding energy, especially for $n = 2$, is close to a phonon resonance. Taking this into account will shift the data point closer to the theoretically expected value. This points to a possible extension of our theory in which a frequency-dependent permittivity could be incorporated in a self-consistent manner by including it both in the Coulomb interaction potential and the Rydberg energy. The observed high-n shift on the other hand may be due to the fact that the measurement setup had to be altered for the resonances beyond $n = 10$. Thus, a small systematic shift might have occurred, which features prominently in the deviation parameter $\alpha_{n,S}$.

Although we have focussed solely on the yellow exciton series of Cu_2O, it is clear that our procedure is valid for all semiconductors that possess both spin-orbit interactions as well as cubic symmetry within their band structure. In particular, we expect the green exciton series of Cu_2O to provide purely negative values for $\alpha_{n,l}$ because the interband coupling results in an increased curvature of the Γ_8^+ valence band.

Acknowledgments

We thank Ch. Uihlein for his suggestion to analyse the data by use of the 2nd derivative. We gratefully acknowledge support by the Collaborative Research Centre SFB 652/3 'Strong correlations in the radiation field' and the International Collaborative Research Centre TRR 160 'Coherent manipulation of interacting spin excitations in tailored semiconductors', both funded by the Deutsche Forschungsgemeinschaft.

[1] J. Frenkel, *On the transformation of light into heat in solids*, Phys. Rev. **37**, 1276 (1931).
[2] G.H. Wannier, *The structure of electronic excitation levels in insulating crystals*, Phys. Rev. **52**, 191 (1937).
[3] N.F. Mott, *The conduction band and ultra-violet absorption of alkali-halide crystals*, Trans. Faraday Soc. **34**, 500 (1938).
[4] C. Uihlein, D. Fröhlich, and R. Kenklies, *Investigation of exciton fine structure in* Cu_2O, Phys. Rev. B **23**, 2731 (1981).
[5] K. Suzuki and J.C. Hensel, *Quantum resonances in the valence bands of germanium*, Phys. Rev. B **9**, 4184 (1974).
[6] M. French, R. Schwartz, H. Stolz, and R. Redmer, *Electronic band structure of* Cu_2O *by spin density functional theory*, J. Phys.: Condensed Matter **21**, 015502 (2009).
[7] E.F. Gross and N.A. Karryjew, *The optical spectrum of the exciton*, Dokl. Akad. Nauk SSSR **84**, 471 (1952).
[8] M. Hayashi and K. Katsuki, *Hydrogen-like absorption spectrum of cuprous oxide*, J. Phys. Soc. Japan **7**, 599 (1952).
[9] E.F. Gross, *Optical spectrum of excitons in the crystal lattice*, Il Nuovo Cimento **4**, 672 (1956).
[10] J. Brandt, D. Fröhlich, C. Sandfort, M. Bayer, H. Stolz, and N. Naka, *Ultranarrow Optical Absorption and Two-Phonon Excitation Spectroscopy of* Cu_2O *Paraexcitons in a High Magnetic Field*, Phys. Rev. Lett. **99**, 217403 (2007).
[11] T. Kazimierczuk, D. Fröhlich, S. Scheel, H. Stolz, and M. Bayer, *Giant Rydberg excitons in the copper oxide* Cu_2O, Nature **514**, 343 (2014).
[12] G.M. Kavoulakis, Y.-C. Chang, and G. Baym, *Fine structure of excitons in* Cu_2O, Phys. Rev. B **55**, 7593 (1997).
[13] A. Chernikov *et al.*, *Exciton Binding Energy and Nonhydrogenic Rydberg Series in Monolayer* WS_2, Phys. Rev. Lett. **113**, 076802 (2014).
[14] Z. Ye *et al.*, *Probing excitonic dark states in single-layer tungsten disulphide*, Nature **513**, 214 (2014).
[15] K. He *et al.*, *Tightly Bound Excitons in Monolayer* WSe_2, Phys. Rev. Lett. **113**, 026803 (2014).
[16] H. Haug and S.W. Koch, *Quantum Theory of the Optical and Electronic Properties of Semiconductors* (World Scientific, Singapore, 2009).

[17] J.M. Luttinger, *Quantum theory of cyclotron resonance in semiconductors*, Phys. Rev. **102**, 1030 (1956).

[18] J. Thewes *et al.*, *Observation of High Angular Momentum Excitons in Cuprous Oxide*, Phys. Rev. Lett. **115**, 027402 (2015).

[19] B. Podolsky and L. Pauling, *The momentum distribution in hydrogen-like atoms*, Phys. Rev. **34**, 109 (1929).

[20] R. Szmytkowski, *Alternative approach to the solution of the momentum-space Schrödinger equation for bound states of the N-dimensional Coulomb problem*, Ann. Phys. (Berlin) **524**, 345 (2012).

[21] D. Schechter, *Theory of shallow acceptor states in Si and Ge*, J. Phys. Chem. Solids **23**, 237 (1962).

[22] A. Baldereschi and N. O. Lipari, *Spherical Model of Shallow Acceptor States in Semiconductors*, Phys. Rev. B **8**, 2697 (1973).

[23] J. Bernholc and S. T. Pantelides, *Theory of binding energies of acceptors in semiconductors*, Phys. Rev. B **15**, 4935 (1977).

[24] M.A. Washington *et al.*, *Spectroscopy of excited yellow exciton states in* Cu_2O *by forbidden resonant Raman scattering*, Phys. Rev. B **15**, 2145 (1977).

[25] C. Carabatos, A. Diffiné, and M. Sieskind, *Contribution à l'étude des bandes fondamentales de vibration du réseau de la cuprite (Cu2O)*, J. Physique **29**, 529 (1968).

[26] P. Dawson, M.M. Hargreave, and G.R. Wilkinson, *The dielectric and lattice vibrational spectrum of cuprous oxide*, J. Phys. Chem. Solids **34**, 2201 (1973).